BioSystems 235 (2024) 105088

Contents lists available at ScienceDirect

BioSystems

journal homepage: www.elsevier.com/locate/biosystems

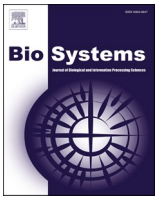

A new mathematical model of folate homeostasis in *E. coli* highlights the potential importance of the folinic acid futile cycle in cell growth

Amy E. Morgan [a,*], J. Enrique Salcedo-Sora [b], Mark T. Mc Auley [c]

[a] School of Health & Sport Sciences, Hope Park, Liverpool Hope University, Liverpool, L16 9JD, UK
[b] Liverpool Shared Research Facilities, GeneMill, University of Liverpool, Liverpool, L69 7ZB, UK
[c] School of Science, Engineering and Environment, University of Salford, Manchester, M5 4NT, UK

ARTICLE INFO

Keywords:
Futile cycle
Folinic acid
Mathematical model
Cell growth
Cell dormancy
Bacteria

ABSTRACT

Folate (vitamin B9) plays a central role in one-carbon metabolism in prokaryotes and eukaryotes. This pathway mediates the transfer of one-carbon units, playing a crucial role in nucleotide synthesis, methylation, and amino acid homeostasis. The folinic acid futile cycle adds a layer of intrigue to this pathway, due to its associations with metabolism, cell growth, and dormancy. It also introduces additional complexity to folate metabolism. A logical way to deal with such complexity is to examine it by using mathematical modelling. This work describes the construction and analysis of a model of folate metabolism, which includes the folinic acid futile cycle. This model was tested under three *in silico* growth conditions. Model simulations revealed: 1) the folate cycle behaved as a stable biochemical system in three growth states (slow, standard, and rapid); 2) the initial concentration of serine had the greatest impact on metabolite concentrations; 3) 5-formyltetrahydrofolate cyclo-ligase (5-FCL) activity had a significant impact on the levels of the 7 products that carry the one-carbon donated from folates, and the redox couple NADP/NADPH; this was particularly evident in the rapid growth state; 4) 5-FCL may be vital to the survival of the cells by maintaining low levels of homocysteine, as high levels can induce toxicity; and 5) the antifolate therapeutic trimethoprim had a greater impact on folate metabolism with higher nutrient availability. These results highlight the important role of 5-FCL in intracellular folate homeostasis and mass generation under different metabolic scenarios.

1. Introduction

Cell growth is a consequence of net biomass gain and a positive energy balance. Under a conducive genetic background, growth is followed by cell multiplication. In microorganisms, biomass gain beyond an intrinsic threshold is followed by cell propagation (Wang and Levin, 2009), via metabolic pathways which are similar across otherwise highly variable species, who inhabit equally diverse environments (Chubukov et al., 2014). Likewise, higher eukaryotes including those that make up complex organisms, have tailored metabolic programmes, to fulfil the needs of rapid cellular proliferation. For instance, a dramatic case of streamlined metabolism for proliferation has been observed in cancer cells (Lunt and Vander Heiden, 2011). In recent years one-carbon folate metabolism (OCFM), has been shown to provide a selective advantage for energy and biomass generation during rapid cell proliferation (Amelio et al., 2014; Locasale, 2013; Yang et al., 2021)). OCFM belongs to a group of enzymatic reactions that condense and interchange a one-carbon unit at different oxidation states (i.e., from formate to methanol) between folates (Tibbetts and Appling, 2010). Folates then transfer this carbon to a crucial number of anabolic reactions for the biosynthesis of DNA precursors (purines and thymidylate), methionine (Met), and formylated methionyl-transfer RNA (fmtRNA) (Kordus and Baughn, 2019).

Beyond these previously known fates of the folate one-carbon intermediates, unexpected links have been discovered between folate and other important molecules of cellular homoeostasis. For example, a genome-scale model of human cell metabolism found that a high metabolite flux through OCFM provided an alternative source of adenosine 5′-triphosphate (ATP) to rapid proliferating cells, when undergoing glycolysis without the net production of ATP (Vazquez et al., 2011). Quantitative metabolic profiling in actively growing cells has also demonstrated that OCFM is a source of NADPH for biomass generation in rapid proliferating cells; in addition to the pathways classically known to fulfil this role (i.e., the pentose phosphate pathway) (Fan et al., 2014).

* Corresponding author.
E-mail address: morgana1@hope.ac.uk (A.E. Morgan).

https://doi.org/10.1016/j.biosystems.2023.105088
Received 17 August 2023; Received in revised form 17 November 2023; Accepted 17 November 2023
Available online 23 November 2023
0303-2647/© 2023 Elsevier B.V. All rights reserved.

Prior to this finding, the gene expression levels of OCFM enzymes have been shown to correlate with high fluxes of ATP and reduced nicotinamide adenine dinucleotide phosphate (NADPH). Moreover, when specific cancer cell lines were treated with antifolates, it was found that ATP levels, AMP kinase activation, ribonucleotides levels, and the synthesis of fatty acids were reduced significantly (Tedeschi et al., 2013). Other investigations have consolidated these metabolic findings. For example, two landmark studies showed that the overexpression of a number of OCFM enzymes drives the proliferation of cancer cells (Jain et al., 2012; Zhang et al., 2012). Furthermore, a number of polymorphisms and epigenetic changes to genes encoding for OCFM enzymes have been reported in a range of cancers (de Castro et al., 2020; Faria et al., 2020; Gustafsson Sheppard et al., 2015; A. E. Morgan et al., 2018; Morgan et al., 2020; Nilsson et al., 2014; Petrone et al., 2021; Usman et al., 2023). Moreover, these mutations have been associated with patient response to chemotherapy (Phillips-Chavez et al., 2021) and prognosis (Luo et al., 2021).

The enzyme 5-formyltetrahydrofolate cyclo-ligase (5-FCL, EC 6.3.3.2) adds particular intrigue to this narrative. The lack of activity of this OCFM enzyme has been shown to reduce cell growth (Field et al., 2007; Stover and Schirch, 1993). The activity of 5-FCL has also been described as a pathogenic factor necessary for antifolate drug resistance in *Mycobacterium* (Ogwang et al., 2011). Conversely, 5-FCL has also been shown to affect the capacity to slow down metabolism in microorganisms that generate dormant cells (persisters), as part of a generic strategy that renders them tolerant to multiple stressors (J. Morgan et al., 2018). The overexpression of 5-FCL has been associated with bacterial dormant phenotypes in liquid cultures (Hansen et al., 2008) as well as in biofilms (Ren et al., 2004). Thus, this enzyme could be part a potential regulatory mechanism seemingly used for both rapid cell growth as well as cell dormancy. Intriguingly, 5-FCL catalyses a reaction that is part of a futile or substrate cycle. Folinic acid is not a substrate for folate biosynthesis, or usage, and is produced as part of this futile cycle only to be recycled back to the folate pool as 5,10-methenyltetrahydrofolate (meTHFGlu) by 5-FCL. Despite this, the bioengineering of bacterial strains which express this gene has been investigated as a means to upregulate the synthesis of the bioactive 5-methyltetrahydrofolate (MTHFGlu), which could be commercially exploited (Lu et al., 2021; Wang et al., 2022). However, futile or substrate cycles are understood to be a mechanism of heat dissipation, since the hydrolysis of ATP is usually involved. Substrate cycles also have the capacity to correct or increase mass generation in a biochemical system with comparably small changes in total flux, a phenomenon denoted as sensitivity (Newsholme et al., 1983).

Other paradigms based on multifaceted metabolic pathways such as aerobic glycolysis (the Warburg effect) and glutaminolysis have facilitated an improved understanding of the behaviour of cell proliferation in cancer (DeBerardinis et al., 2007, 2008; Locasale and Cantley, 2011; Warburg, 1956), normal rapid proliferative mammalian cells (Aït-Ali et al., 2015; De Bock et al., 2013), and microorganisms (Salcedo-Sora et al., 2014). Moreover, due to its inherent ability to represent complex biochemical systems, mathematical modelling has been able to improve our understanding of folate metabolism (Duncan et al., 2013; Luebeck et al., 2008; Mc Auley et al., 2018; Misselbeck et al., 2017, 2019; Morrison and Allegra, 1989; Neuhouser et al., 2011; Nijhout et al., 2004, 2006; Panetta et al., 2013; Reed et al., 2006; Salcedo-Sora and Mc Auley, 2016; Thiaville et al., 2016). However, a model of OCFM that integrates recent biochemical information from cell proliferation studies, and includes folinic acid as a metabolite, while also considering the substrate availability, is lacking. This work uses mathematical modelling as a means of integrating this information into a cohesive network. This framework permitted the dynamics of this complex system to be quantitatively explored. Using this methodology, three different biochemical scenarios involving the folate cycle were examined. These deterministic simulations are underpinned by kinetic data, and have been assembled with the inclusion of folinic acid as a key metabolite, together with the reactions of the futile cycle that this metabolite is part of. Moreover, the model is capable of representing the kinetic behaviour of this substrate cycle, and how it mediates the production of biomass and redox equivalents to provide a selective advantage in cellular growth. The model is also an ideal theoretical framework for exploring the proposed involvement of folinic acid metabolism in both slow growth and quiescence/dormancy in microorganisms. In addition, it can also be used to investigate faster modes of growth driven by nutrient abundance.

2. Methods

2.1. Network diagram

A network diagram of the model was developed using the systems biology graphical notation (SBGN) process descriptions (PD) language in the open-source software VANTED V2.8.7 (Fig. 1) (Junker et al., 2006). The process diagram includes the folate cycle and the production and salvage of folinic acid (5-formyltetrahydrofolate, ffTHFGlu). Specifically, the folate intermediates carry a one-carbon unit at either of three levels of oxidation: formate (10-Formyltetrahydrofolate (fTHFGlu), ffTHFGlu, meTHFGlu), formaldehyde (5,10-Methylenetetrahydrofolate, myTHFGlu), or methanol (MTHFGlu). Anabolic products from the reactions fed by MTHFGlu and myTHFGlu produce methionine (Met) and thymidine monophosphate (dTMP) in reactions R8 and R10, respectively. fTHFGlu serves the reactions that generate 1-(5′-phosphoribosyl)-5-formamido-4-imidazolecarboxamide (FAICAR), 5′-phosphor ibosyl-*n*-formylglycinamide (FGAR), and the mitochondrial or bacterial fmtRNA, in reactions R22, R20, and R15. Importantly, fTHFGlu can also generate NADPH and carbon dioxide (CO_2) when fully oxidised (R17). Similarly, the one-carbon unit can be released as formate using this free energy to condense a molecule of ATP (R14). Conversely, meTHFGlu, which is not a direct substrate of any of these anabolic reactions nor a precursor of reductive or energy equivalents, has previously been included in the folate cycle only as an intermediate in the reversible oxidation of myTHFGlu to fTHFGlu (R12 and R13). In this mathematical model the published experimental data (Anguera et al., 2003; Huang and Schirch, 1995; Stover and Schirch, 1990; Tolley et al., 2012) is taken into account, and the model includes meTHFGlu as the precursor for a futile or substrate cycle (R18 and R19).

2.2. Model assembly and parameterisation

Once the SBGN-PD diagram was constructed, the network was translated into a series of reactions and assembled in the open-source modelling and simulation software tool COPASI version 4.39.272 (Hoops et al., 2006). The model consists of 39 species across 23 reactions. Model species and reactions are defined in Tables S1 and S2 (supplementary file S1) respectively. Within the model, 20 of the 39 species were fixed. These were limited to co-reactants and sink species. Specifically, these species were: adenosine 5′-diphosphate (ADP), 1-(5′-phosphoribosyl)-5-amino-4 -imidazolecarboxamide (AICAR), ATP, CO_2, deoxyuridine 5′-phosphate (dUMP), formyl, 5′-phosphoribosylglycinamide (GAR), L-Glutamate (Glu), Glycine (Gly), L-homocysteine (Hcy), nicotinamide adenine dinucleotide (NAD), reduced nicotinamide adenine dinucleotide (NADH), ammonia (NH_3), phosphate (Pi), L-serine (Ser), sink_dTMP, sink_FAICAR, sink_FGAR, sink_fmtRNA, and Sink_Met. Reaction parameter values are outlined in Table S3 (supplementary file S1). A list of ordinary differential equations (ODEs) can be found in supplementary file S2. The components of the model are informed by some of the existing kinetic models of folate metabolism (Nijhout et al., 2004; Salcedo-Sora and Mc Auley, 2016), and relevant reviews of microbial folate metabolism (de Crécy-Lagard, 2014; Salcedo-Sora and Ward, 2013). Moreover, a number of microbial metabolic representations as archived within the KEGG database (Kyoto encyclopaedia of genes and genomes http://www.genome.jp/kegg/) were considered (Kanehisa and Goto, 2000) based on the comparative genomics from the hundreds of microbial genomes sequenced to date (Koonin and Wolf, 2008).

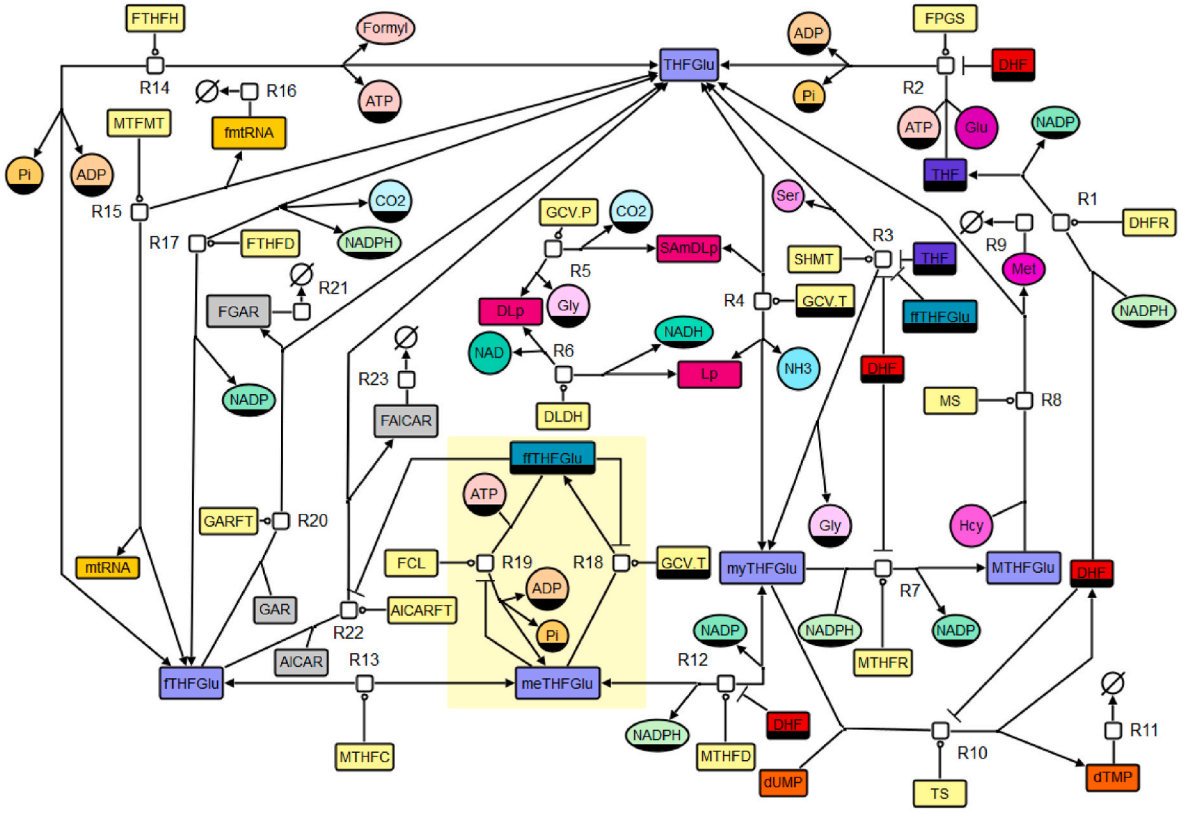

Fig. 1. SBGN-PD network diagram of the folate cycle, including the folinic acid futile cycle. The species and reactions are outlined in Tables S1 and S2 of supplementary file S1. Arrows represent flux, rounded arrows represent catalysis and T-shaped arrows represent inhibition. The mathematical symbol for an empty set represents a biochemical source or sink. The folinic acid futile cycle is represented by reactions 18 and 19, highlighted in yellow. Abbreviations are as follows: AICAR: 1-(5′-Phosphoribosyl)-5-amino-4-imidazolecarboxamide; DHF: Dihydrofolate; DLp: Dihydrolipoylprotein ([H Protein]-dihydrolipoyllysine), dTMP: Deoxythymidine 5′-phosphate; dUMP: Deoxyuridine 5′-phosphate; FAICAR: 1-(5′-Phosphoribosyl)-5-formamido-4-imidazolecarboxamide; ffTHFGLU: 5-formyltetrahydrofolate; FGAR: 5′-Phosphoribosyl-*N*-formylglycinamide; fmtRNA: *N*-Formylmethionyl-tRNA; fTHFGLU: 10-Formyltetrahydrofolate; GAR: 5′-Phosphoribosylglycinamide; Glu: L-Glutamate; Gly: Glycine; Hcy: L-Homocysteine; Lp: Lipoylprotein ([H Protein]-lipoyllysine); Met: L-Methionine; METHFGLU: 5,10-Methenyltetrahydrofolate; MTHFGLU: 5-Methyltetrahydrofolate; mtRNA: L-Methionyl-tRNA; myTHFGLU: 5,10-Methylenetetrahydrofolate; SAmDLp: *S*-Aminomethyldihydrolipoylprotein (H-Protein-*S*-aminomethyldihydrolipoyllysine); Ser: L-Serine; THF: Tetrahydrofolate; THFGLU: THF-polyglutamate(n).

A time course analysis was conducted using the deterministic (LSODA) method. As outlined in Fig. 2, when simulated the species concentrations converged to equilibrium values (240 min). The equilibrium point of the model was asymptotically stable at a resolution of 1×10^{-9}. Following construction and analysis, the model was converted to Systems Biology Markup Language (SBML), an interchangeable file format. This model was deposited in BioModels (Malik-Sheriff et al., 2020) and assigned the identifier MODEL2308150001.

3. Results

3.1. Examination of the folate cycle under three different initial sets of metabolite concentrations

Accumulating evidence indicates that OCFM is involved in phenotypes associated with slow metabolism (e.g., persisters to antibiotics) as well as in rapid cell growth (Fan et al., 2014; Field et al., 2007; Gustafsson Sheppard et al., 2015; Hansen et al., 2008; Jain et al., 2012;

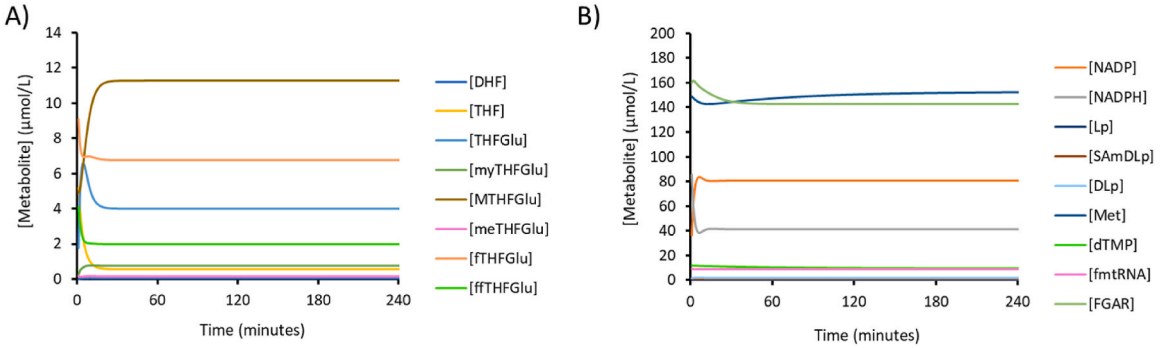

Fig. 2. Time course analysis. Time course analysis of A) the eight folate metabolites (DHF, ffTHFGlu, fTHFGlu, meTHFGlu, MTHFGlu, myTHFGlu, THF, THFGlu) and B) the seven products (DLp, SAmDLp, dTMP, FAICAR, FGAR, fmtRNA, and Met) that carry the one-carbon donated from folates, plus the reductive equivalents NADP and NADPH, over 240 min.

Nilsson et al., 2014; Ogwang et al., 2011; Ren et al., 2004; Stover and Schirch, 1993; Tedeschi et al., 2013; Vazquez et al., 2011; Yang et al., 2021; Zhang et al., 2012; Zhu and Thompson, 2019). It was therefore deemed biologically cogent to investigate the impact of differing initial metabolite availability on cell growth. Specifically, three states were investigated. Each state is characterised by distinct initial concentrations (at t = 0 min) of substrates for energy, anabolic reactions and reductive equivalents: AICAR, ATP, dihydrofolate (DHF), dUMP, GAR, Glu, Gly, Hcy, L-methionyl-tRNA (mtRNA), nicotinamide adenine dinucleotide phosphate (NADP), and Ser. The standard state retains the standard set of known experimental initial values for these species (Bennett et al., 2009), while the slow and rapid states are simulated by increasing or decreasing the initial values of these metabolites by two orders of magnitude (Table 1). The scales of these different initial concentrations reflect the range of experimentally observed metabolite concentrations that can affect cell growth rate proportionally to nutrient availability (Boer et al., 2010; Tepper et al., 2013). Specifically, the model captures a range of metabolites expected at different growing phases in a bacterial cell such as the concentrations previously measured for central carbon metabolism in *E. coli*. Those have been shown to expand three orders of magnitude and above (Yamamotoya et al., 2012). The lowest scale ($\times 10^{-2}$) in particular captures the realistic level of nutrients encountered by bacteria in natural environments where scarcity is the norm. Hence, the evolution of survival mechanisms for low nutrient availability, such as the stringent response (Barik, 2023). Previous models of the one-carbon folate metabolism built quantitatively different metabolite levels with similar ranges for a virtual eukaryotic cell population. Those levels were based on distributions of folate and homocysteine in the plasma and tissues as found in the National Health and Nutrition Examination Survey (NHANES) data (Duncan et al., 2013).

Results were analysed at 240 min as this was the time it took for the standard model to reach equilibrium. Interestingly, it was noted that while the slow model converges to equilibrium at t = 240 min (4 h), the rapid model converged at t = 25 min, the approximate doubling time of *E. coli*. Under slow growth conditions the model reached equilibrium at approximately t = 800 min (13 h).

Summation of the species concentration was used as a proxy indicator for total mass. Total mass is represented by 15 folate metabolites (folate mass) and NADP/NADPH, which were not fixed in the model. The folate mass represents the eight metabolites (DHF, ffTHFGlu, fTHFGlu, meTHFGlu, MTHFGlu, myTHFGlu, tetrahydrofolate (THF), THF-polyglutamate(n) (THFGlu)) that originated from folic acid, which share the pterin and *para*-aminobenzoate rings as DHF or THF (Salcedo-Sora and Ward, 2013) plus the seven products (Dihydrolipoylprotein ([H Protein]-dihydrolipoyllysine (DLp), *S*-aminomethyldihydrolipoy lprotein (H-protein-*s*-aminomethyldihydrolipoyllysine) (SAmDLp), dTMP, FAICAR, FGAR, fmtRNA, and Met) that carry the one-carbon unit donated from folates. When the 11 substrates were adjusted, the initial total mass of the 15 folate metabolites in the slow, standard and rapid states were 478.67, 480.77 and 691.35. At 240 min, total mass was calculated as 174.09, 486.22 and 1077.00 in the slow, standard and rapid states, respectively. There was little change up to 1000 min (169.31, 486.58 and 1084.68). Importantly, when breaking down the composition of the total folate mass, the eight folate metabolites between the three states (25.44, 25.47 and 28.14) were similar at 240 min. Conversely, a significant difference was observed with the seven products which carry one-carbon donated from folates (28.63, 338.65 and 718.85) and NADP/NADPH (120.02, 122.10 and 333.00) across the three growth states. Interestingly, the ratio of the redox couple NADP/NADPH was significantly affected by this simulation. In the standard state, NADP/NADPH were in a ratio of ~2:1 at 240 min. In the rapid model this ratio was adjusted to ~1:6, and in the slow state this was ~585:1. It is important to note that disruption to redox homeostasis can result in oxidative or reductive stress which can be detrimental to cell functioning (Xiao et al., 2018).

Table 1
Initial metabolite values for the slow, standard and rapid state simulations. Metabolite concentrations are in μmol/L.

Metabolite	Growth State		
	Slow	Standard	Rapid
AICAR	1.35	135	13,500
ATP	96	9600	960,000
DHF	0.00027	0.027	2.7
dUMP	0.1	10	1000
GAR	5.64	564	56,400
Glu	9600	960,000	96,000,000
Gly	4.3	430	43,000
Hcy	3.7	370	37,000
mtRNA	0.001003	1.003	100.3
NADP	0.021	2.1	210
Ser	0.68	68	6800

3.2. Parameter scan of initial metabolite concentrations

To examine the impact of variations to the initial concentration of these 11 metabolites independently, a parameter scan was conducted. In each instance, three values for each metabolite (AICAR, ATP, DHF, dUMP, GAR, Glu, Gly, Hcy, mtRNA, NADP, and Ser) were examined. These are the standard value, and values two orders of magnitude greater and less than this value (Table 1). Species concentrations were recorded at 240 min (Table S4, supplementary file S1). In most cases, species directly related to the scanned metabolite were affected most dramatically by changes in the initial concentration. For example, when the standard value for AICAR was retained, FAICAR was 22.67 μmol/L after 240 min. A two orders of magnitude increase or decrease in this species resulted in FAICAR rising to 34.81 μmol/L or lowering to 0.62 μmol/L (R22). Likewise, when mtRNA, GAR, and NADP were investigated, fmtRNA, FGAR, and NADPH were the species most significantly affected respectively (R15, R20, and R1/7/12/17). Interestingly, the initial concentration of serine had the greatest impact on metabolite concentrations (R3). Specifically, the product THFGlu decreased from 22.37 μmol/min to 1.03 μmol/min, while myTHFGlu rose from 0.2 μmol/min to 0.96 μmol/min when the initial concentration of serine was 2 orders of magnitude lower and higher than the standard value. Downstream metabolites such as THF, MTHFGlu, meTHFGlu and ffTHFGlu were also affected by this change in the initial concentration of serine.

In human melanoma it has been shown that serine synthesis is upregulated, with a significant proportion converted to glycine (Kit, 1955). Furthermore, glycine has been shown to increase the rate of growth (0.67 vs 0.78 h^{-1}) and cell yield (0.57 vs. 0.78 g dry weight per g substrate) in *E. coli* (Han et al., 2002). When the impact of elevated glycine was investigated, a small increase in myTHFGlyu and MTHFGlu was observed. This contrasts with the finding from the mathematical model of Misselbeck et al. (2019) who reported that elevated intracellular glycine resulted in serine synthesis, and thus myTHFGly and MTHFGlu depletion (Misselbeck et al., 2019). In this simulation, SAmDLp, DLp, and lipoylprotein ([H Protein]-lipoyllysine) (Lp) were the three most affected metabolites when glycine was perturbed, although when the total of these 3 metabolites were investigated, no change was observed. In addition to myTHFGly and MTHFGlu, other key folate metabolites/products such as THF, NADPH, methionine were elevated.

3.3. Global analysis of initial metabolite concentrations

Next, a global analysis was conducted to gain further insight into the relationship between initial metabolite concentrations and folate mass. A global parameter scan can determine the impact of variations in a number of parameters or species simultaneously; which may represent

real-world conditions more accurately. In this case, 500 random samples were taken using a uniform distribution over a range of two orders of magnitude higher and lower than the standard initial value of each of the adjusted 11 metabolites. A uniform distribution was chosen due to a lack of *priori* data (Marino et al., 2008). Although many initial concentrations were derived from experimental work which used *E. coli*, several concentrations were derived from alternative models. Specifically, AICAR and GAR were derived from murine leukaemia cells (Sant et al., 1992), Gly was gained from *Plasmodium falciparum* (Teng et al., 2009), and DHF and mtRNA were derived from mathematical models. Therefore, it was deemed prudent to use the uniform distribution between a large range of initial concentrations (Marino et al., 2008), which reflected the range of experimentally observed metabolite concentrations (Boer et al., 2010; Tepper et al., 2013).

Eight metabolites were analysed (DHF, ffTHFGlu, fTHFGlu, meTHFGlu, MTHFGlu, myTHFGlu, THF, THFGlu) after 240 min, with results depicted relative to serine. Serine was chosen as the metabolite of interest as it provoked the greatest changes in folate metabolites. In each case, the concentration of the folate metabolite appeared to increase up to approximately 500 μmol/L of serine. After this, serine had little

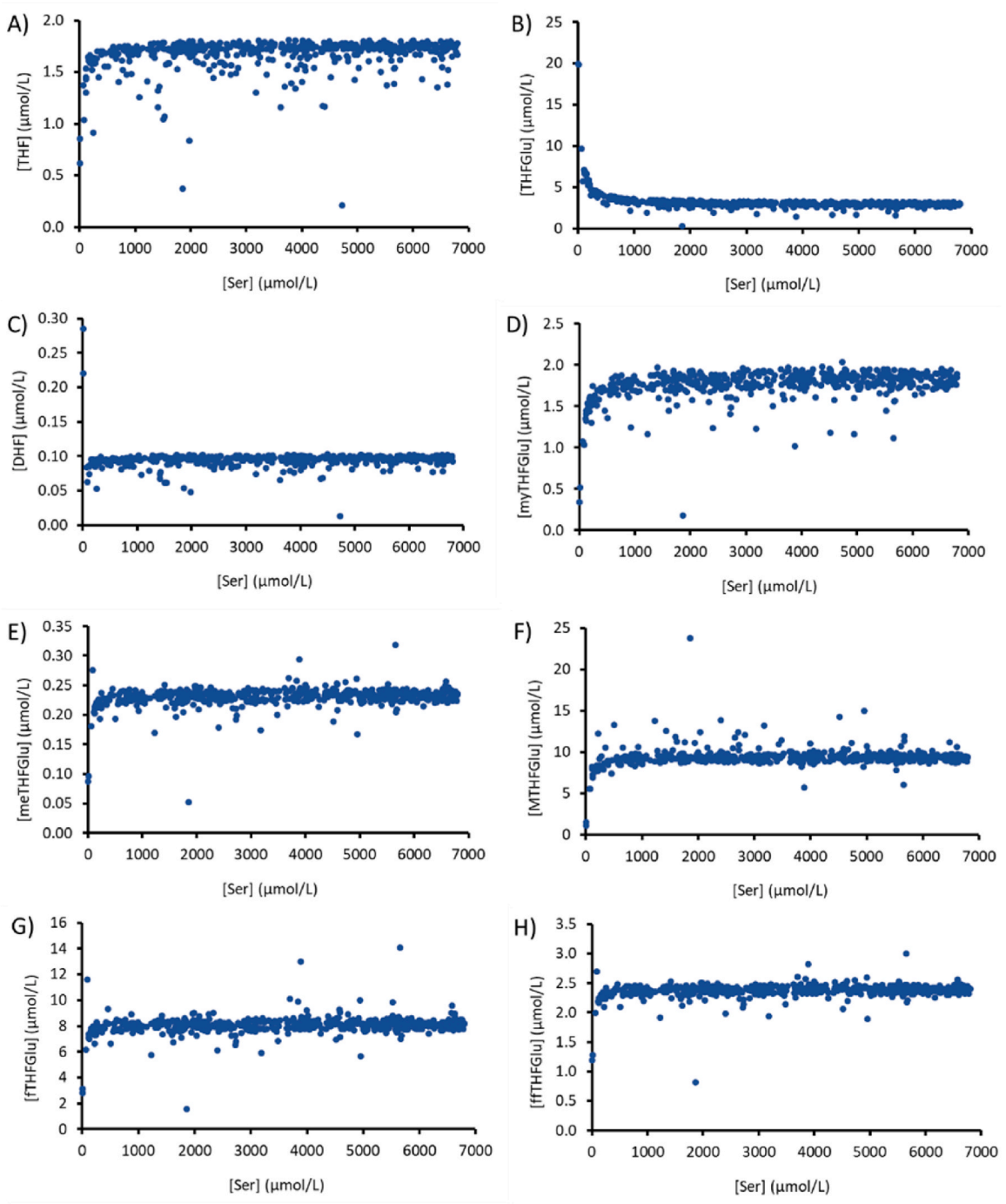

Fig. 3. Global parameter scan of AICAR, ATP, DHF, dUMP, GAR, Glu, Gly, Hcy, mtRNA, NADP, and Ser, and the impact on the eight metabolites that originate from folic acid. The eight metabolites are A) THF, B) THFGlu, C) DHF, D) myTHFGlu, E) meTHFGlu, F) MTHFGlu, G) fTHFGlu, and H) ffTHFGlu. Initial concentrations were scanned between values 2 orders of magnitude greater than and less than the initial values. Random samples were taken using a uniform distribution at 240 min (n = 500).

impact on the concentration of the metabolite (Fig. 3). THF did not increase beyond 1.82 μmol/L. THFGlu and DHF did not increase beyond 19.98 μmol/L and 0.28 μmol/L, although most values laid between 2 and 4 μmol/L and 0.08–0.1 μmol/L respectively. The global analysis determined that when all of the initial concentrations of these species were altered, greatest variation was observed with NADPH after 240 min (Fig. S1, supplementary file S1). Values ranged from 0.41 to 280.02 μmol/L, with equal distribution. Similarly, NADP exhibited a spread between values of 0.24 and 279.41 μmol/L. However in this case, most values were between 48 and 52 μmol/L when serine was >500 μmol/L. Met also exhibited a diverse range of concentrations, although at serine values > 500 μmol/L most values were situated between 300 and 350 μmol/L.

3.4. Parameter scan of 5-FCL

5,10-Methenyltetrahydrofolate (meTHFGlu) can be oxidised to 5-formyl-THFGlu (ffTHFGlu, folinic acid) as part of a hydrolysis reaction (reaction R18). However, 5-formyl-THFGlu (ffTHFGlu), is not a substrate for any anabolic reactions of the folate cycle. On the contrary, ffTHFGlu is only known to be converted back to meTHFGlu in an ATP-driven reaction catalysed by 5-formyltetrahydrofolate cyclo-ligase (5-FCL, EC 6.3.3.2, also named methenyltetrahydrofolate synthetase) (Huang and Schirch, 1995). Therefore, these two reactions are part of a futile cycle within the folate cycle. Experimental data suggest that 5-FCL, in addition to OCFM, are involved in dormancy and rapid cell growth (Fan et al., 2014; Field et al., 2007; Gustafsson Sheppard et al., 2015; Hansen et al., 2008; Jain et al., 2012; Nilsson et al., 2014; Ogwang et al., 2011; Stover and Schirch, 1990, 1993; Tedeschi et al., 2013; Vazquez et al., 2011; Zhang et al., 2012). Thus, it was relevant to investigate the role this enzyme has on metabolites across the three growth states. To do this, the V_{max} for reaction 19 (V_{max19}) was scanned between the values of 0 and 40 μmol/min with an interval size of 2 (standard value = 20 μmol/min). Results at 240 min are presented in Fig. 4. As V_{max19} increased, ffTHFGlu decreased and meTHFGlu increased in all three growth states. This is logical as V_{max19} represents the maximum velocity of the enzyme 5-FCL, which catalyses the conversion of ffTHFGlu to meTHFGlu. This is also in line with the findings from an extended hybrid-stochastic model of OCFM which determined that a 50% reduction in this enzyme resulted in an increase in ffTHFGlu and a decrease in meTHFGlu (Misselbeck et al., 2019).

This model was able to shed light on OFCM in *E. coli* by evaluating the role of 5-FCL in different growth states. Specifically, it was determined that the increase in meTHFGlu observed with greater 5-FCL activity, was more pronounced in the rapid state. Furthermore, simulation of a 5-FCL knockout resulted in the accumulation of ffTHFGlu, particularly in the rapid model. Specifically, ffTHFGlu was 10.17 μmol/L, 21.03 μmol/L and 24.77 μmol/L in the slow, standard and rapid states respectively when V_{max19} was 0 μmol/min. Similarly, the 5-FCL knockout simulation resulted in reduced levels of meTHFGlu which were more pronounced in the slow model (slow: 0.0062 μmol/L, standard: 0.038 μmol/L, and rapid: 0.042 μmol/L). Likewise, THF, THFGlu, myTHFGlu, MTHFGlu, and fTHFGlu were reduced when a 5-FCL knockout was simulated. Surprisingly, DHF was elevated in the knockout model under standard growth conditions, although they were reduced in both the slow and rapid states. Conversely, Misselbeck et al. (2019) demonstrated that DHF was unchanged when 5-FCL activity was decreased to 50%, but reduced to 0 μM in the knockout simulation.

An increase in V_{max19} was associated with an increase in myTHFGlu, DHF, THF, and MTHFGlu, which slowed with advancing maximum velocity. Similarly, it has been demonstrated experimentally that overexpression of the *fau* gene encoding for 5-FCL resulted in a significant decrease in ffTHFGlu and a 32% increase in MTHFGlu in *Lactococcus lactis* (Lu et al., 2021). Simulations indicated that in a slow growth state, the increase in myTHFGlu, THF, MTHFGlu, and DHF was less pronounced when compared to the standard and rapid growth states. Despite these changes in folate species, total folate mass remained relatively constant at V_{max19} values between 0 and 40 μmol/min in all three model states (25.44, 25.47 and 28.14 in the slow, standard and rapid states respectively) indicating that homeostasis in overall folate was maintained in a variety of growth conditions despite changes in 5-FCL activity. However, there was a significant difference observed in the seven products that carry the one-carbon donated from folates and the redox couple NADP/NADPH. For instance, in the slow state, total mass of these metabolites increased from 134.04 at a V_{max19} value of 0 μmol/min, to 150.35 at a V_{max19} value of 40 μmol/min. A more profound increase was observed in the standard (183.24–474.72) and rapid states (512.67–1096.45).

3.5. Simulation of trimethoprim treatment

The antifolate trimethoprim is a potent inhibitor of bacterial dihydrofolate reductase (DHFR), the enzyme responsible for the conversion of DHF to THF (R1) (Wróbel et al., 2020). Importantly, 61–78% of *E. coli* isolates have been shown to be susceptible to trimethoprim (Duployez et al., 2018; Kawalec et al., 2023; Rosello et al., 2017; Somorin et al., 2022). Interestingly, experimental evidence on the impact of nutrient availability on antibiotic susceptibility/cell survival is conflicting (Ortiz-Severín et al., 2021; Thorfinnsdottir et al., 2023). To simulate trimethoprim treatment in the model, a parameter scan of the V_{max} of R1 was conducted. The standard value of 38.33 μmol/min was deemed to represent 100% enzyme function. In total 11 values were scanned. This represented 10% increments in enzyme function from 0 to 100%. For instance, a value of 3.83 μmol/min represented 10% function, or 90% inhibition in enzyme activity, while a value of 19.17 μmol/min represented a 50% decline in activity. The simulated trimethoprim treatment had a greater impact on folate metabolism with more nutrient availability after 240 min (Fig. 5). Significantly, many of the species were relatively unresponsive at lower levels of DHFR inhibition. A 5.59% reduction in total mass after 90% DHFR inhibition and a 42.5%

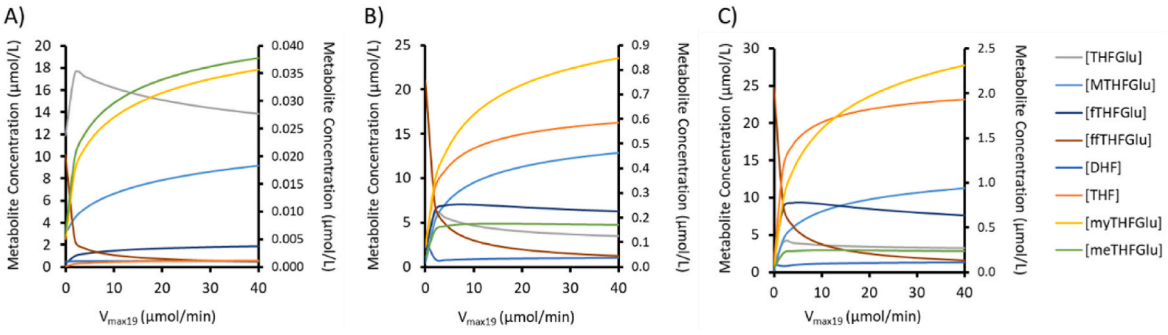

Fig. 4. Impact of perturbations to the maximum velocity (V_{max}) of the enzyme 5-FCL (R19, V_{max19}) on folate metabolites under A) slow, B) standard, and C) rapid growth states.

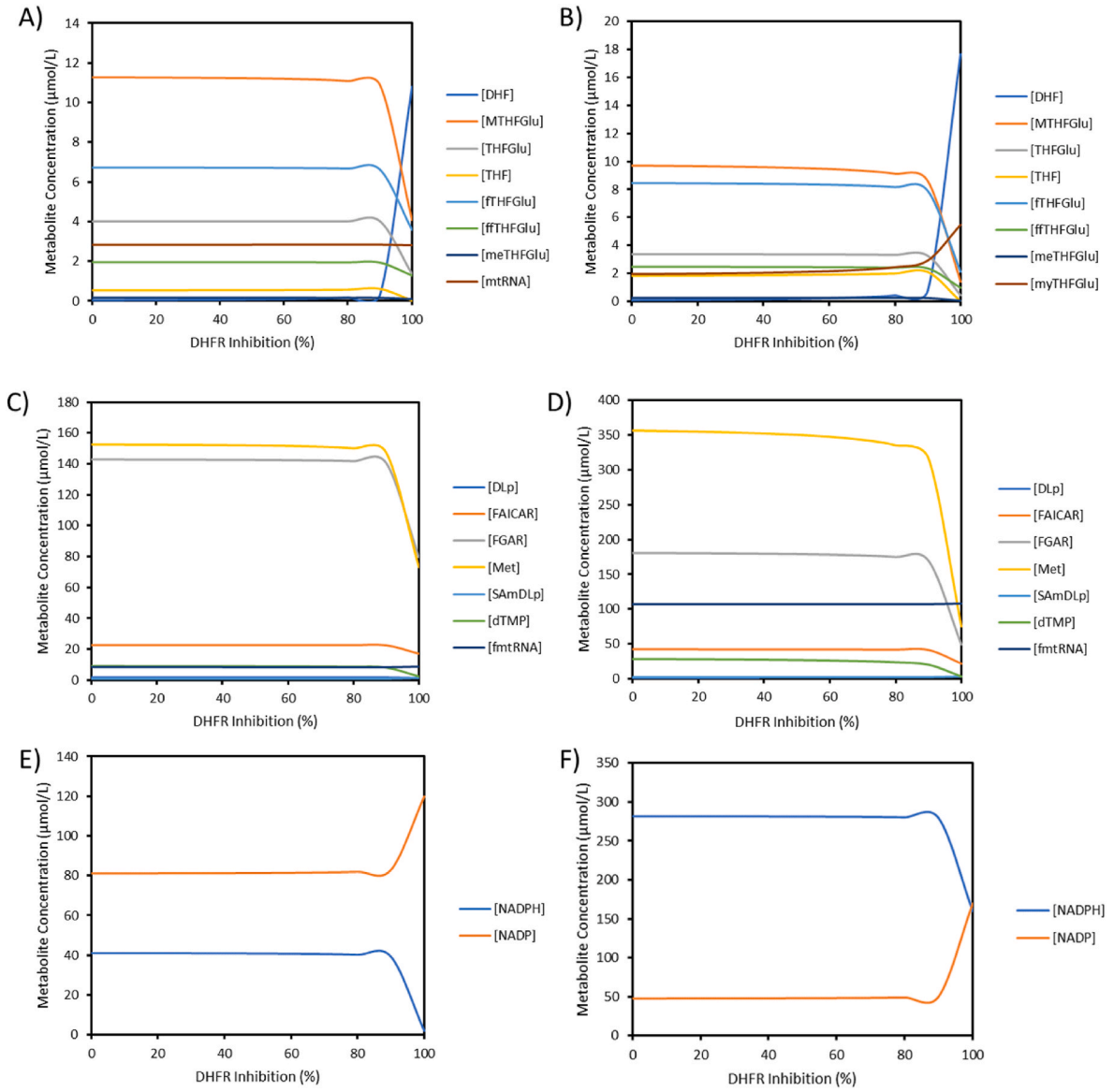

Fig. 5. Impact of Trimethoprim treatment on folate metabolism. Effect of DHFR inhibition on the eight folate metabolites (DHF, ffTHFGlu, fTHFGlu, meTHFGlu, MTHFGlu, myTHFGlu, THF, THFGlu) (A and B), the seven products (DLp, SAmDLp, dTMP, FAICAR, FGAR, fmtRNA, and Met) that carry the one-carbon donated from folates (C and D), and the reductive equivalents NADP and NADPH (E and F), over 240 min in the standard (A, C and E) and rapid growth states (B, D and F).

reduction following DHFR knockout was observed in the rapid growth state after 240 min. Total DHFR inhibition led to a rise in DHF from 0.1 µmol/L (100% activity) to 17.69 µmol/L, and a subsequent decline in THFGlu, from 3.37 µmol/min to 0.41 µmol/min. Interestingly, the greatest impact was observed in the 7 products that carry the one-carbon unit donated from folates, with methionine, FGAR, FAICAR and dTMP associated with a 4.7-, 3.7-, 2.0, and 9.6-fold reduction respectively. Similar, although smaller, changes were observed in the standard model. Specifically, 90% enzyme inhibition resulted in a 1.78% reduction in total mass; 100% inhibition resulted in a 31.75% reduction. Total inhibition resulted in DHF rising from 0.03 µmol/min to 10.80 µmol/min, and THFGlu reducing from 4.00 µmol/min to 1.34 µmol/min. There was limited change in overall mass (−0.0015%) with complete inhibition of DHFR in the slow model (Fig. S2, supplementary file S1).

3.6. Sensitivity analysis

To better understand the sensitivity of species to reaction parameters, a sensitivity analysis was conducted in COPASI (supplementary file S3). When analysing V_{max19} in the scaled sensitivities array, the most sensitive species were fmtRNA (5930.32) and mtRNA (5929.75). The unscaled sensitivities array indicated that methionine (1.65) was most sensitive to perturbations in V_{max19}, followed by FGAR (−0.57), FAICAR (0.39), and NADP (−0.33).

3.7. Metabolic control analysis

A metabolic control analysis was conducted (supplementary file S4) to investigate the control that enzymes exert on the flux of reactions. The unscaled flux control coefficient indicated that perturbations in 5-FCL, the enzyme that catalyses reaction 19, had the greatest, and equal, impact on the flux of reactions 22 and 23 (10.63). Next, the flux of reaction 3 was affected most greatly (5.76). This was followed by the flux of reactions 12 and 13 (4.67). Next, the flux of R20 and 21 were most greatly affected (−1.56), and following this, reactions 7, 8, and 9 (0.65). It is interesting that these sequential reactions have equal flux control coefficients. This may indicate that in this system, the first reaction (e.g., R22, R20, R7) may be rate limiting in this part of the model. These

findings may also indicate that 5-FCL plays a role in maintaining low levels of homocysteine (Hcy). Methionine synthase (MS) catalyses MTHFGlu and Hcy to THFGlu and Met. The positive value of the flux control coefficient indicates that lowering the enzymatic activity of 5-FCL may lead to reduced flux of this reaction, thus leading to an accumulation of Hcy. This may be vital to the survival of the cells as high levels of Hcy can induce toxicity (Hasan et al., 2019; Tuite et al., 2005).

To further understand the metabolic control of the model, the concentration control coefficients were analysed. This analysis indicates the impact of perturbed enzymes on model species. The unscaled concentration coefficient analysis revealed that Met was most greatly affected (44.69) by perturbations in the enzyme controlling reaction 19. This was followed by FGAR (−15.56). However, in this case, the concentration control coefficient was negative, indicating that as the activity of 5-FCL increases, FGAR declines. The scaled concentration coefficient analysis indicated that ffTHFFlu was most greatly affected (−0.63). This is expected as 5-FCL catalyses the conversion of ffTHFFlu to meTHFGlu. This is followed by FAICAR (0.35). This is also expected as ffTHFGlu inhibits AICARFT, the enzyme responsible for the conversion of fTHFGlu and AICAR to THFGlu and FAICAR. Therefore, increased 5-FCL should lower the concentration of ffTHFGlu, thus causing a reduction in AICARFT inhibition. Third, fourth, and fifth were myTHFGlu (0.226), THFGlu (−0.219) and MTHGlu (0.217). Sixth was met (0.216). This supports the findings from the flux control analysis, where it was shown that 5-FCL exerts force over R8 where Hcy is converted to methionine.

Methylenetetrahydrofolate reductase (MTHFR) catalyses the reduction of myTHFGlu to MTHFGlu (Leclerc et al., 2013). In humans, deficiency of this enzyme has been associated with hyper-homo cysteinaemia, which has been linked with cardiovascular disease, thrombosis, cognitive impairment and complications of pregnancy, amongst other conditions (Moll and Varga, 2015). The effect of the key enzyme MTHFR (R7) on reaction flux and species levels was also investigated. The flux analysis indicated that reaction 17 was most affected (2.37), followed by R20 and R21 (−2.21). Next, R12 and R13 were impacted (−1.91). Following this, R3 (−1.17). This indicates that as MTHFR activity increases, flux from THFGlu and Ser to myTHFGlu and Gly declines. This is in line with the findings from a hybrid stochastic model of OCFM (Misselbeck et al., 2017) and hybrid stochastic model of OCFM (Misselbeck et al., 2019). Misselbeck et al. (2017) suggested that decreased MTHFR activity reduced MTHFGlu. This was observed in this work through analysis of the concentration control coefficients. It was revealed that MTHFR (R7) exerted control over MTHFGlu, with an unscaled concentration coefficient of 2.45 and a scaled concentration coefficient of 0.48.

4. Discussion

Folate metabolism is a densely interconnected network of metabolic pathways that include the *de novo* synthesis of THFGlu in prokaryotes and plants. From this hub metabolite, several usage pathways evolved in both prokaryotes and eukaryotes. These include: conversion of serine and glycine, the cyclic methylation of homocysteine to methionine, production of *N*-formylmethionyl-tRNA and the *de novo* synthesis of purine/dTMP (Kordus and Baughn, 2019). Experimental work has continued to substantiate a case for folate metabolism as a driving fource of cell mass and proliferation, through the biosynthesis of chemical energy and reductive equivalents in the form of ATP and NADPH, respectively (Fan et al., 2014; Gustafsson Sheppard et al., 2015; Jain et al., 2012; Nilsson et al., 2014; Tedeschi et al., 2013; Vazquez et al., 2011; Zhang et al., 2012). Principally, the enzyme that salvages ffTHFGlu (folinic acid), 5-FCL, has specifically been shown to affect cell growth phenotypes (i.e. dormancy versus rapid cell proliferation) (Field et al., 2007; Hansen et al., 2008; Ogwang et al., 2011; Ren et al., 2004; Salcedo-Sora and Mc Auley, 2016; Stover and Schirch, 1993). Folinic acid is generated enzymatically only to be converted back to meTHFGlu (Field et al., 2007; Salcedo et al., 2005; Stover and Schirch, 1993). These two reactions are referred to as a futile or substrate cycle. However, this aspect of OCFM remains to be widely acknowledged. Enzymatic futile cycles represent a recurring control motif in biological molecular networks, appearing in a wide variety of processes from energy metabolism to signal transduction.

There can be significant variation in the folate biosynthesis pathways among different bacterial species. This variation can affect their ability to synthesize folate and influence their survival and growth in different environments. Here, mathematical modelling was used to investigate the behaviour of the folate cycle and the folinic acid futile cycle. Different initial substrate concentrations were selected as proxies for different modes of cell growth and proliferation. This mathematical model (supplementary file S5) and the results generated have furthered our understanding of the mechanisms whereby folate metabolism modulates cell mass and proliferation. In this work, a complex metabolic network was assembled; this consisted of coupled ODEs, informed by Michaelis-Menten kinetics derived from the extensive experimental literature in this area (Nijhout et al., 2004; Salcedo-Sora and Mc Auley, 2016). Also, where there is experimental support, negative feedback loops were included within the reactions. The folinic acid futile cycle contains the parameters which have been derived from three decades of experimental work in this area (Anguera et al., 2003; Bennett et al., 2009; Huang and Schirch, 1995; Stover and Schirch, 1990). The only assumptions inherent to this model are the different initial concentrations for the substrates of the anabolic reactions (i.e., AICAR, DHF, dUMP, GAR, Glu, Gly, Hcy, mtRNA, Ser) as well as for NADP and ATP. The standard initial conditions comprise initial metabolite concentrations as reported for the majority of these entities in a prokaryotic model fed with glucose (Bennett et al., 2009). The rapid and slow initial states represented metabolite concentrations two orders of magnitude above and below the standard initial conditions. This reflected the range of nutrient availability that can affect cell growth rate (Boer et al., 2010; Tepper et al., 2013).

Output from the mathematical model is in close alignment with the experimental data which shows that gene knock-out (KO) mutants of 5-FCL in bacteria are affected in their capacity to develop the antibiotic persister phenotype (dormancy or slow growth) (Hansen et al., 2008; J. Morgan et al., 2018). For example, in a 5-FCL KO strain of *E. coli*, only ~13% of the persisters to antibiotics were generated compared to the isogenic control. Similarly, the same 5-FCL mutants are able to proliferate only up to 75% of the control (J. Morgan et al., 2018). This model suggests that this may be due to the interplay between one-carbon folate metabolism and NADPH production. The latter is part of the known interplay between folate metabolism and the oxidative pentose-phosphate pathway (Chen et al., 2019).

The model also demonstrated the impact antifolate antimicrobials can have on the folate metabolism pathway and cell growth. Metabolic models continue to support antibiotic research and drug repurposing, particularly in combinatorial antibacterials, where folate biosynthesis inhibition sensitises the cell to other forms of toxicity (Chen et al., 2022). Similarly, in our previous mathematical model, the inhibition of the bifunctional enzyme dihydrofolate synthase-folylpolyglutamate synthase (DHFS-FPGS) showed a highly synergistic effect with inhibitors of dihydrofolate reductase (DHFR) – of which there are several clinically deployed (Salcedo-Sora and Mc Auley, 2016). The latter example of synergistic cell toxicity mediated by folate biosynthesis inhibition was corroborated by the experimental findings from a group of DHFS-FPGS inhibitors tested against intracellular pathogens (Wang et al., 2010). The model presented here offers a new critical potential target in 5-FCL. Inhibitors of this enzyme could have the capacity of severely impairing cell multiplication. 5-FCL is shown here to connect the folinic acid futile cycle, mediating cell mass generation, with folate cell mass biosynthesis and NADP/NADPH homeostasis.

Many previous models have not included the folinic acid cycle which is a futile cycle in biochemical terms. The model has shown how the folate biosynthesis and usage pathways in a model *E. coli* cell behaves in

the presence of this futile cycle. This more complete model should inform research fields such as those of antifolate discovery, antibiotic resistance, and synergistic antibacterial research (Chen et al., 2022).

5. Conclusion

A theoretical framework is presented for the biochemical folate biosynthesis and usage pathways including the folinic acid futile cycle. The relevance of this new model was tested with different parameters that aimed at representing relevant growth phenotypes. The inclusion of the folinic acid futile cycle within the model highlighted the important roles this cycle seems to play in modulating flux and mass generation under proliferation during different metabolic scenarios. These findings have important implications for antibiotic research and antifolate chemotherapy (i.e., cancer research).

Funding

This research did not receive any specific grant from funding agencies in the public, commercial, or not-for-profit sectors.

CRediT authorship contribution statement

Amy E. Morgan: Data curation, Formal analysis, Investigation, Methodology, Project administration, Resources, Validation, Visualization, Writing – original draft, Writing – review & editing. **J. Enrique Salcedo-Sora:** Conceptualization, Data curation, Formal analysis, Investigation, Methodology, Project administration, Resources, Writing – original draft, Writing – review & editing. **Mark T. Mc Auley:** Conceptualization, Investigation, Methodology, Writing – original draft, Writing – review & editing.

Declaration of competing interest

The authors declare that they have no known competing financial interests or personal relationships that could have appeared to influence the work reported in this paper.

Acknowledgements

The authors would like to thank their respective institutions for the support provided during this work.

Appendix A. Supplementary data

Supplementary data to this article can be found online at https://doi.org/10.1016/j.biosystems.2023.105088.

References

Aït-Ali, N., Fridlich, R., Millet-Puel, G., Clérin, E., Delalande, F., Jaillard, C., Blond, F., Perrocheau, L., Reichman, S., Byrne, L.C., Olivier-Bandini, A., Bellalou, J., Moyse, E., Bouillaud, F., Nicol, X., Dalkara, D., van Dorsselaer, A., Sahel, J.-A., Léveillard, T., 2015. Rod-derived cone viability factor promotes cone survival by stimulating aerobic glycolysis. Cell 161, 817–832. https://doi.org/10.1016/j.cell.2015.03.023.

Amelio, I., Cutruzzolá, F., Antonov, A., Agostini, M., Melino, G., 2014. Serine and glycine metabolism in cancer. Trends Biochem. Sci. 39, 191–198. https://doi.org/10.1016/j.tibs.2014.02.004.

Anguera, M.C., Suh, J.R., Ghandour, H., Nasrallah, I.M., Selhub, J., Stover, P.J., 2003. Methenyltetrahydrofolate synthetase regulates folate turnover and accumulation. J. Biol. Chem. 278, 29856–29862. https://doi.org/10.1074/jbc.M302883200.

Barik, S., 2023. Protein-ligand interactions in scarcity: the stringent response from bacteria to metazoa, and the unanswered questions. Int. J. Mol. Sci. 24, 3999. https://doi.org/10.3390/ijms24043999.

Bennett, B.D., Kimball, E.H., Gao, M., Osterhout, R., Van Dien, S.J., Rabinowitz, J.D., 2009. Absolute metabolite concentrations and implied enzyme active site occupancy in Escherichia coli. Nat. Chem. Biol. 5, 593–599. https://doi.org/10.1038/nchembio.186.

Boer, V.M., Crutchfield, C.A., Bradley, P.H., Botstein, D., Rabinowitz, J.D., 2010. Growth-limiting intracellular metabolites in yeast growing under diverse nutrient limitations. Mol. Biol. Cell 21, 198–211. https://doi.org/10.1091/mbc.E09-07-0597.

Chen, L., Zhang, Z., Hoshino, A., Zheng, H.D., Morley, M., Arany, Z., Rabinowitz, J.D., 2019. NADPH production by the oxidative pentose-phosphate pathway supports folate metabolism. Nat. Metab. 1, 404–415.

Chen, P.-H., Sung, L.-K., Hegemann, J.D., Chu, J., 2022. Disrupting transcription and folate biosynthesis leads to synergistic suppression of Escherichia coli growth. ChemMedChem 17, e202200075. https://doi.org/10.1002/cmdc.202200075.

Chubukov, V., Gerosa, L., Kochanowski, K., Sauer, U., 2014. Coordination of microbial metabolism. Nat. Rev. Microbiol. 12, 327–340. https://doi.org/10.1038/nrmicro3238.

De Bock, K., Georgiadou, M., Schoors, S., Kuchnio, A., Wong, B.W., Cantelmo, A.R., Quaegebeur, A., Ghesquière, B., Cauwenberghs, S., Eelen, G., Phng, L.-K., Betz, I., Tembuyser, B., Brepoels, K., Welti, J., Geudens, I., Segura, I., Cruys, B., Bifari, F., Decimo, I., Blanco, R., Wyns, S., Vangindertael, J., Rocha, S., Collins, R.T., Munck, S., Daelemans, D., Imamura, H., Devlieger, R., Rider, M., Van Veldhoven, P. P., Schuit, F., Bartrons, R., Hofkens, J., Fraisl, P., Telang, S., Deberardinis, R.J., Schoonjans, L., Vinckier, S., Chesney, J., Gerhardt, H., Dewerchin, M., Carmeliet, P., 2013. Role of PFKFB3-driven glycolysis in vessel sprouting. Cell 154, 651–663. https://doi.org/10.1016/j.cell.2013.06.037.

de Castro, T.B., Rodrigues-Fleming, G.H., de Oliveira-Cucolo, J.G., da Silva, J.N.G., Silva, F.P., Raposo, L.S., Maniglia, J.V., Pavarino, É.C., Arantes, L.M.R.B., Galbiatti-Dias, A.L.S., Goloni-Bertollo, E.M., 2020. Gene polymorphisms involved in folate metabolism and DNA methylation with the risk of head and neck cancer. Asian Pac. J. Cancer Prev. APJCP 21, 3751–3759. https://doi.org/10.31557/APJCP.2020.21.12.3751.

de Crécy-Lagard, V., 2014. Variations in metabolic pathways create challenges for automated metabolic reconstructions: examples from the tetrahydrofolate synthesis pathway. Comput. Struct. Biotechnol. J. 10, 41–50. https://doi.org/10.1016/j.csbj.2014.05.008.

DeBerardinis, R.J., Lum, J.J., Hatzivassiliou, G., Thompson, C.B., 2008. The biology of cancer: metabolic reprogramming fuels cell growth and proliferation. Cell Metabol. 7, 11–20. https://doi.org/10.1016/j.cmet.2007.10.002.

DeBerardinis, R.J., Mancuso, A., Daikhin, E., Nissim, I., Yudkoff, M., Wehrli, S., Thompson, C.B., 2007. Beyond aerobic glycolysis: transformed cells can engage in glutamine metabolism that exceeds the requirement for protein and nucleotide synthesis. Proc. Natl. Acad. Sci. U. S. A. 104, 19345–19350. https://doi.org/10.1073/pnas.0709747104.

Duncan, T.M., Reed, M.C., Nijhout, H.F., 2013. A population model of folate-mediated one-carbon metabolism. Nutrients 5, 2457–2474. https://doi.org/10.3390/nu5072457.

Duployez, C., Robert, J., Vachée, A., Onerba, 2018. Trimethoprim susceptibility in E. coli community-acquired urinary tract infections in France. Med. Maladies Infect. 48, 410–413. https://doi.org/10.1016/j.medmal.2018.03.010.

Fan, J., Ye, J., Kamphorst, J.J., Shlomi, T., Thompson, C.B., Rabinowitz, J.D., 2014. Quantitative flux analysis reveals folate-dependent NADPH production. Nature 510, 298–302. https://doi.org/10.1038/nature13236.

Faria, G.M., Soares, I.D.P., D'Alincourt Salazar, M., Amorim, M.R., Pessoa, B.L., da Fonseca, C.O., Quirico-Santos, T., 2020. Intranasal perillyl alcohol therapy improves survival of patients with recurrent glioblastoma harboring mutant variant for MTHFR rs1801133 polymorphism. BMC Cancer 20, 294. https://doi.org/10.1186/s12885-020-06802-8.

Field, M.S., Szebenyi, D.M.E., Perry, C.A., Stover, P.J., 2007. Inhibition of 5,10-methenyltetrahydrofolate synthetase. Arch. Biochem. Biophys. 458, 194–201. https://doi.org/10.1016/j.abb.2006.12.023.

Gustafsson Sheppard, N., Jarl, L., Mahadessian, D., Strittmatter, L., Schmidt, A., Madhusudan, N., Tegnér, J., Lundberg, E.K., Asplund, A., Jain, M., Nilsson, R., 2015. The folate-coupled enzyme MTHFD2 is a nuclear protein and promotes cell proliferation. Sci. Rep. 5, 15029 https://doi.org/10.1038/srep15029.

Han, L., Doverskog, M., Enfors, S.-O., Häggström, L., 2002. Effect of glycine on the cell yield and growth rate of Escherichia coli: evidence for cell-density-dependent glycine degradation as determined by 13C NMR spectroscopy. J. Biotechnol. 92, 237–249. https://doi.org/10.1016/S0168-1656(01)00373-X.

Hansen, S., Lewis, K., Vulić, M., 2008. Role of global regulators and nucleotide metabolism in antibiotic tolerance in Escherichia coli. Antimicrob. Agents Chemother. 52, 2718–2726. https://doi.org/10.1128/AAC.00144-08.

Hasan, T., Arora, R., Bansal, A.K., Bhattacharya, R., Sharma, G.S., Singh, L.R., 2019. Disturbed homocysteine metabolism is associated with cancer. Exp. Mol. Med. 51, 1–13. https://doi.org/10.1038/s12276-019-0216-4.

Hoops, S., Sahle, S., Gauges, R., Lee, C., Pahle, J., Simus, N., Singhal, M., Xu, L., Mendes, P., Kummer, U., 2006. COPASI–a COmplex PAthway SImulator. Bioinformatics 22, 3067–3074. https://doi.org/10.1093/bioinformatics/btl485.

Huang, T., Schirch, V., 1995. Mechanism for the coupling of ATP hydrolysis to the conversion of 5-formyltetrahydrofolate to 5,10-methenyltetrahydrofolate. J. Biol. Chem. 270, 22296–22300. https://doi.org/10.1074/jbc.270.38.22296.

Jain, M., Nilsson, R., Sharma, S., Madhusudhan, N., Kitami, T., Souza, A.L., Kafri, R., Kirschner, M.W., Clish, C.B., Mootha, V.K., 2012. Metabolite profiling identifies a key role for Glycine in rapid cancer cell proliferation. Science 336, 1040–1044. https://doi.org/10.1126/science.1218595.

Junker, B.H., Klukas, C., Schreiber, F., 2006. VANTED: a system for advanced data analysis and visualization in the context of biological networks. BMC Bioinf. 7, 109. https://doi.org/10.1186/1471-2105-7-109.

Kanehisa, M., Goto, S., 2000. KEGG: kyoto encyclopedia of genes and genomes. Nucleic Acids Res. 28, 27–30.

Kawalec, A., Józefiak, J., Kiliś-Pstrusińska, K., 2023. Urinary tract infection and antimicrobial resistance patterns: 5-year experience in a tertiary pediatric nephrology center in the southwestern region of Poland. Antibiotics (Basel) 12, 1454. https://doi.org/10.3390/antibiotics12091454.

Kit, S., 1955. The biosynthesis of free glycine and serine by tumors. Cancer Res. 15, 715–718.
Koonin, E.V., Wolf, Y.I., 2008. Genomics of bacteria and archaea: the emerging dynamic view of the prokaryotic world. Nucleic Acids Res. 36, 6688–6719. https://doi.org/10.1093/nar/gkn668.
Kordus, S.L., Baughn, A.D., 2019. Revitalizing antifolates through understanding mechanisms that govern susceptibility and resistance. Medchemcomm 10, 880–895. https://doi.org/10.1039/c9md00078j.
Leclerc, D., Sibani, S., Rozen, R., 2013. Molecular biology of methylenetetrahydrofolate reductase (MTHFR) and overview of mutations/polymorphisms. In: Madame Curie Bioscience Database. Landes Bioscience [Internet].
Locasale, J.W., 2013. Serine, glycine and one-carbon units: cancer metabolism in full circle. Nat. Rev. Cancer 13, 572–583. https://doi.org/10.1038/nrc3557.
Locasale, J.W., Cantley, L.C., 2011. Metabolic flux and the regulation of mammalian cell growth. Cell Metabol. 14, 443–451. https://doi.org/10.1016/j.cmet.2011.07.014.
Lu, C., Liu, Y., Li, J., Liu, L., Du, G., 2021. Engineering of biosynthesis pathway and NADPH supply for improved L-5-methyltetrahydrofolate production by Lactococcus lactis. J. Microbiol. Biotechnol. 31, 154. https://doi.org/10.4014/jmb.1910.10069.
Luebeck, E.G., Moolgavkar, S.H., Liu, A.Y., Boynton, A., Ulrich, C.M., 2008. Does folic acid supplementation prevent or promote colorectal cancer? Results from model-based predictions. Cancer Epidemiol. Biomarkers Prev. 17, 1360–1367. https://doi.org/10.1158/1055-9965.EPI-07-2878.
Lunt, S.Y., Vander Heiden, M.G., 2011. Aerobic glycolysis: meeting the metabolic requirements of cell proliferation. Annu. Rev. Cell Dev. Biol. 27, 441–464. https://doi.org/10.1146/annurev-cellbio-092910-154237.
Luo, L., Zheng, Y., Lin, Z., Li, Xiaodi, Li, Xiaoling, Li, M., Cui, L., Luo, H., 2021. Identification of SHMT2 as a potential prognostic biomarker and correlating with immune infiltrates in lung adenocarcinoma. J Immunol Res 2021, 6647122. https://doi.org/10.1155/2021/6647122.
Malik-Sheriff, R.S., Glont, M., Nguyen, T.V.N., Tiwari, K., Roberts, M.G., Xavier, A., Vu, M.T., Men, J., Maire, M., Kananathan, S., Fairbanks, E.L., Meyer, J.P., Arankalle, C., Varusai, T.M., Knight-Schrijver, V., Li, L., Dueñas-Roca, C., Dass, G., Keating, S.M., Park, Y.M., Buso, N., Rodriguez, N., Hucka, M., Hermjakob, H., 2020. BioModels-15 years of sharing computational models in life science. Nucleic Acids Res. 48, D407–D415. https://doi.org/10.1093/nar/gkz1055.
Marino, S., Hogue, I.B., Ray, C.J., Kirschner, D.E., 2008. A methodology for performing global uncertainty and sensitivity analysis in systems biology. J. Theor. Biol. 254, 178–196. https://doi.org/10.1016/j.jtbi.2008.04.011.
Mc Auley, M.T., Mooney, K.M., Salcedo-Sora, J.E., 2018. Computational modelling folate metabolism and DNA methylation: implications for understanding health and ageing. Briefings Bioinf. 19, 303–317. https://doi.org/10.1093/bib/bbw116.
Misselbeck, K., Marchetti, L., Field, M.S., Scotti, M., Priami, C., Stover, P.J., 2017. A hybrid stochastic model of folate-mediated one-carbon metabolism: effect of the common C677T MTHFR variant on de novo thymidylate biosynthesis. Sci. Rep. 7, 797. https://doi.org/10.1038/s41598-017-00854-w.
Misselbeck, K., Marchetti, L., Priami, C., Stover, P.J., Field, M.S., 2019. The 5-formyl-tetrahydrofolate futile cycle reduces pathway stochasticity in an extended hybrid-stochastic model of folate-mediated one-carbon metabolism. Sci. Rep. 9, 4322. https://doi.org/10.1038/s41598-019-40230-4.
Moll, S., Varga, E.A., 2015. Homocysteine and MTHFR mutations. Circulation 132. https://doi.org/10.1161/CIRCULATIONAHA.114.013311 e6–e9.
Morgan, A.E., Acutt, K.D., Mc Auley, M.T., 2020. Electrochemically detecting DNA methylation in the EN1 gene promoter: implications for understanding ageing and disease. Biosci. Rep. 40 https://doi.org/10.1042/BSR20202571. BSR20202571.
Morgan, A.E., Davies, T.J., Auley, M.T.M., 2018. The role of DNA methylation in ageing and cancer. Proc. Nutr. Soc. 77, 412–422. https://doi.org/10.1017/S0029665118000150.
Morgan, J., Smith, M., Mc Auley, M.T., Enrique Salcedo-Sora, J., 2018. Disrupting folate metabolism reduces the capacity of bacteria in exponential growth to develop persisters to antibiotics. Microbiology 164, 1432–1445. https://doi.org/10.1099/mic.0.000722.
Morrison, P.F., Allegra, C.J., 1989. Folate cycle kinetics in human breast cancer cells. J. Biol. Chem. 264, 10552–10566.
Neuhouser, M.L., Nijhout, H.F., Gregory III, J.F., Reed, M.C., James, S.J., Liu, A., Shane, B., Ulrich, C.M., 2011. Mathematical modeling predicts the effect of folate deficiency and excess on cancer-related biomarkers. Cancer Epidemiol. Biomarkers Prev. 20, 1912. https://doi.org/10.1158/1055-9965.EPI-10-1352. –1917.
Newsholme, E.A., Arch, J.R., Brooks, B., Surholt, B., 1983. The role of substrate cycles in metabolic regulation. Biochem. Soc. Trans. 11, 52–56. https://doi.org/10.1042/bst0110052.
Nijhout, H.F., Reed, M.C., Budu, P., Ulrich, C.M., 2004. A mathematical model of the folate cycle: new insights into folate homeostasis. J. Biol. Chem. 279, 55008–55016. https://doi.org/10.1074/jbc.M410818200.
Nijhout, H.F., Reed, M.C., Lam, S.-L., Shane, B., Gregory, J.F., Ulrich, C.M., 2006. In silico experimentation with a model of hepatic mitochondrial folate metabolism. Theor. Biol. Med. Model. 3, 40. https://doi.org/10.1186/1742-4682-3-40.
Nilsson, R., Jain, M., Madhusudhan, N., Sheppard, N.G., Strittmatter, L., Kampf, C., Huang, J., Asplund, A., Mootha, V.K., 2014. Metabolic enzyme expression highlights a key role for MTHFD2 and the mitochondrial folate pathway in cancer. Nat. Commun. 5, 3128. https://doi.org/10.1038/ncomms4128.
Ogwang, S., Nguyen, H.T., Sherman, M., Bajaksouzian, S., Jacobs, M.R., Boom, W.H., Zhang, G.-F., Nguyen, L., 2011. Bacterial conversion of folinic acid is required for antifolate resistance. J. Biol. Chem. 286, 15377 https://doi.org/10.1074/jbc.M111.231076.
Ortiz-Severín, J., Stuardo, C.J., Jiménez, N.E., Palma, R., Cortés, M.P., Maldonado, J., Maass, A., Cambiazo, V., 2021. Nutrient scarcity in a new defined medium reveals metabolic resistance to antibiotics in the fish pathogen piscirickettsia salmonis. Front. Microbiol. 12.
Panetta, J.C., Paugh, S.W., Evans, W.E., 2013. Mathematical Modeling of Folate Metabolism, vol. 5. Wiley Interdiscip Rev Syst Biol Med, pp. 603–613. https://doi.org/10.1002/wsbm.1227.
Petrone, I., Bernardo, P.S., dos Santos, E.C., Abdelhay, E., 2021. MTHFR C677T and A1298C polymorphisms in breast cancer, gliomas and gastric cancer: a review. Genes 12, 587. https://doi.org/10.3390/genes12040587.
Phillips-Chavez, C., Coward, J., Watson, M., Schloss, J., 2021. A retrospective cross-sectional cohort trial assessing the prevalence of MTHFR polymorphisms and the influence of diet on platinum resistance in ovarian cancer patients. Cancers 13, 5215. https://doi.org/10.3390/cancers13205215.
Reed, M.C., Nijhout, H.F., Neuhouser, M.L., Gregory, J.F., Shane, B., James, S.J., Boynton, A., Ulrich, C.M., 2006. A mathematical model gives insights into nutritional and genetic aspects of folate-mediated one-carbon metabolism. J. Nutr. 136, 2653–2661. https://doi.org/10.1093/jn/136.10.2653.
Ren, D., Bedzyk, L.A., Thomas, S.M., Ye, R.W., Wood, T.K., 2004. Gene expression in Escherichia coli biofilms. Appl. Microbiol. Biotechnol. 64, 515–524. https://doi.org/10.1007/s00253-003-1517-y.
Rosello, A., Hayward, A.C., Hopkins, S., Horner, C., Ironmonger, D., Hawkey, P.M., Deeny, S.R., 2017. Impact of long-term care facility residence on the antibiotic resistance of urinary tract Escherichia coli and Klebsiella. J. Antimicrob. Chemother. 72, 1184–1192. https://doi.org/10.1093/jac/dkw555.
Salcedo, E., Sims, P.F.G., Hyde, J.E., 2005. A glycine-cleavage complex as part of the folate one-carbon metabolism of Plasmodium falciparum. Trends Parasitol. 21, 406–411. https://doi.org/10.1016/j.pt.2005.07.001.
Salcedo-Sora, J.E., Caamano-Gutierrez, E., Ward, S.A., Biagini, G.A., 2014. The proliferating cell hypothesis: a metabolic framework for Plasmodium growth and development. Trends Parasitol. 30, 170–175. https://doi.org/10.1016/j.pt.2014.02.001.
Salcedo-Sora, J.E., Mc Auley, M.T., 2016. A mathematical model of microbial folate biosynthesis and utilisation: implications for antifolate development. Mol. Biosyst. 12, 923–933. https://doi.org/10.1039/c5mb00801h.
Salcedo-Sora, J.E., Ward, S.A., 2013. The folate metabolic network of Falciparum malaria. Mol. Biochem. Parasitol. 188, 51–62. https://doi.org/10.1016/j.molbiopara.2013.02.003.
Sant, M.E., Lyons, S.D., Phillips, L., Christopherson, R.I., 1992. Antifolates induce inhibition of amido phosphoribosyltransferase in leukemia cells. J. Biol. Chem. 267, 11038–11045. https://doi.org/10.1016/S0021-9258(19)49872-4.
Somorin, Y.M., Weir, N.-J.M., Pattison, S.H., Crockard, M.A., Hughes, C.M., Tunney, M. M., Gilpin, D.F., 2022. Antimicrobial resistance in urinary pathogens and culture-independent detection of trimethoprim resistance in urine from patients with urinary tract infection. BMC Microbiol. 22, 144. https://doi.org/10.1186/s12866-022-02551-9.
Stover, P., Schirch, V., 1993. The metabolic role of leucovorin. Trends Biochem. Sci. 18, 102–106. https://doi.org/10.1016/0968-0004(93)90162-g.
Stover, P., Schirch, V., 1990. Serine hydroxymethyltransferase catalyzes the hydrolysis of 5,10-methenyltetrahydrofolate to 5-formyltetrahydrofolate. J. Biol. Chem. 265, 14227–14233. https://doi.org/10.1016/S0021-9258(18)77290-6.
Tedeschi, P.M., Markert, E.K., Gounder, M., Lin, H., Dvorzhinski, D., Dolfi, S.C., Chan, L. L.-Y., Qiu, J., DiPaola, R.S., Hirshfield, K.M., Boros, L.G., Bertino, J.R., Oltvai, Z.N., Vazquez, A., 2013. Contribution of serine, folate and glycine metabolism to the ATP, NADPH and purine requirements of cancer cells. Cell Death Dis. 4, e877. https://doi.org/10.1038/cddis.2013.393.
Teng, R., Junankar, P.R., Bubb, W.A., Rae, C., Mercier, P., Kirk, K., 2009. Metabolite profiling of the intraerythrocytic malaria parasite Plasmodium falciparum by 1H NMR spectroscopy. NMR Biomed. 22, 292–302. https://doi.org/10.1002/nbm.1323.
Tepper, N., Noor, E., Amador-Noguez, D., Haraldsdóttir, H.S., Milo, R., Rabinowitz, J., Liebermeister, W., Shlomi, T., 2013. Steady-state metabolite concentrations reflect a balance between maximizing enzyme efficiency and minimizing total metabolite load. PLoS One 8, e75370. https://doi.org/10.1371/journal.pone.0075370.
Thiaville, J.J., Frelin, O., García-Salinas, C., Harrison, K., Hasnain, G., Horenstein, N.A., Díaz de la Garza, R.I., Henry, C.S., Hanson, A.D., de Crécy-Lagard, V., 2016. Experimental and metabolic modeling evidence for a folate-cleaving side-activity of ketopantoate hydroxymethyltransferase (PanB). Front. Microbiol. 7, 431. https://doi.org/10.3389/fmicb.2016.00431.
Thorfinnsdottir, L.B., Bø, G.H., Booth, J.A., Bruheim, P., 2023. Survival of Escherichia coli after high-antibiotic stress is dependent on both the pregrown physiological state and incubation conditions. Front. Microbiol. 14.
Tibbetts, A.S., Appling, D.R., 2010. Compartmentalization of Mammalian folate-mediated one-carbon metabolism. Annu. Rev. Nutr. 30, 57–81. https://doi.org/10.1146/annurev.nutr.012809.104810.
Tolley, M., Bickford, L., Clare, K., Johann, T.W., 2012. Investigations of amino acids in the ATP binding site of 5,10-methenyltetrahydrofolate synthetase. Protein J. 31, 519–528. https://doi.org/10.1007/s10930-012-9428-3.
Tuite, N.L., Fraser, K.R., O'Byrne, C.P., 2005. Homocysteine toxicity in Escherichia coli is caused by a perturbation of branched-chain amino acid biosynthesis. J. Bacteriol. 187, 4362–4371. https://doi.org/10.1128/JB.187.13.4362-4371.2005.
Usman, M., Hameed, Y., Ahmad, M., Iqbal, M.J., Maryam, A., Mazhar, A., Naz, S., Tanveer, R., Saeed, H., Bint-E-Fatima, Ashraf, A., Hadi, A., Hameed, Z., Tariq, E., Aslam, A.S., 2023. SHMT2 is associated with tumor purity, CD8+ T immune cells infiltration, and a novel therapeutic target in four different human cancers. Curr. Mol. Med. 23, 161–176. https://doi.org/10.2174/1566524022666220112142409.
Vazquez, A., Markert, E.K., Oltvai, Z.N., 2011. Serine biosynthesis with one carbon catabolism and the glycine cleavage system represents a novel pathway for ATP generation. PLoS One 6, e25881. https://doi.org/10.1371/journal.pone.0025881.

Wang, J.D., Levin, P.A., 2009. Metabolism, cell growth and the bacterial cell cycle. Nat. Rev. Microbiol. 7, 822–827. https://doi.org/10.1038/nrmicro2202.

Wang, P., Wang, Q., Yang, Y., Coward, J.K., Nzila, A., Sims, P.F.G., Hyde, J.E., 2010. Characterisation of the bifunctional dihydrofolate synthase-folylpolyglutamate synthase from Plasmodium falciparum; a potential novel target for antimalarial antifolate inhibition. Mol. Biochem. Parasitol. 172, 41–51. https://doi.org/10.1016/j.molbiopara.2010.03.012.

Wang, Y., Zhang, M., Li, L., Yi, J., Liang, J., Wang, S., Xu, P., 2022. Biosynthesis of L-5-methyltetrahydrofolate by genetically engineered Escherichia coli. Microb. Biotechnol. 15, 2758–2772. https://doi.org/10.1111/1751-7915.14139.

Warburg, O., 1956. On the origin of cancer cells. Science 123, 309–314. https://doi.org/10.1126/science.123.3191.309.

Wróbel, A., Arciszewska, K., Maliszewski, D., Drozdowska, D., 2020. Trimethoprim and other nonclassical antifolates an excellent template for searching modifications of dihydrofolate reductase enzyme inhibitors. J. Antibiot. 73, 5–27. https://doi.org/10.1038/s41429-019-0240-6.

Xiao, W., Wang, R.-S., Handy, D.E., Loscalzo, J., 2018. NAD(H) and NADP(H) redox couples and cellular energy metabolism. Antioxidants Redox Signal. 28, 251–272. https://doi.org/10.1089/ars.2017.7216.

Yamamotoya, T., Dose, H., Tian, Z., Fauré, A., Toya, Y., Honma, M., Igarashi, K., Nakahigashi, K., Soga, T., Mori, H., Matsuno, H., 2012. Glycogen is the primary source of glucose during the lag phase of E. coli proliferation. Biochim. Biophys. Acta 1824, 1442–1448. https://doi.org/10.1016/j.bbapap.2012.06.010.

Yang, C., Zhang, J., Liao, M., Yang, Y., Wang, Y., Yuan, Y., Ouyang, L., 2021. Folate-mediated one-carbon metabolism: a targeting strategy in cancer therapy. Drug Discov. Today 26, 817–825. https://doi.org/10.1016/j.drudis.2020.12.006.

Zhang, W.C., Shyh-Chang, N., Yang, H., Rai, A., Umashankar, S., Ma, S., Soh, B.S., Sun, L. L., Tai, B.C., Nga, M.E., Bhakoo, K.K., Jayapal, S.R., Nichane, M., Yu, Q., Ahmed, D. A., Tan, C., Sing, W.P., Tam, J., Thiruganam, A., Noghabi, M.S., Pang, Y.H., Ang, H.S., Mitchell, W., Robson, P., Kaldis, P., Soo, R.A., Swarup, S., Lim, E.H., Lim, B., 2012. Glycine decarboxylase activity drives non-small cell lung cancer tumor-initiating cells and tumorigenesis. Cell 148, 259–272. https://doi.org/10.1016/j.cell.2011.11.050.

Zhu, J., Thompson, C.B., 2019. Metabolic regulation of cell growth and proliferation. Nat. Rev. Mol. Cell Biol. 20, 436–450. https://doi.org/10.1038/s41580-019-0123-5.